International Journal of Applied Earth Observations and Geoinformation 106 (2022) 102658

Contents lists available at ScienceDirect

International Journal of Applied Earth Observations and Geoinformation

journal homepage: www.elsevier.com/locate/jag

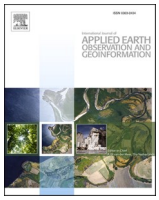

Integrating terrestrial laser scanning and unmanned aerial vehicle photogrammetry to estimate individual tree attributes in managed coniferous forests in Japan

Katsuto Shimizu [a,*], Tomohiro Nishizono [a], Fumiaki Kitahara [a], Keiko Fukumoto [b], Hideki Saito [a]

[a] Department of Forest Management, Forestry and Forest Products Research Institute, 1 Matsunosato, Tsukuba, Ibaraki 305-8687, Japan
[b] Shikoku Research Center, Forestry and Forest Products Research Institute, 2-915 Asakuranishi, Kochi 780-8077, Japan

ARTICLE INFO

Keywords:
Structure from Motion
Planted forest
Integration
UAV

ABSTRACT

The accurate estimation of tree attributes is essential for sustainable forest management. Terrestrial Laser Scanning (TLS) is a viable remote sensing technology suitable for estimating under canopy structure. However, TLS measurements generally underestimate tree height in taller trees, which leads to the underestimation of other tree attributes (e.g., stem volume). The integration of information derived from TLS and Unmanned Aerial Vehicle (UAV) photogrammetry could potentially improve tree height estimation. This study investigated the applicability of integrating TLS and UAV photogrammetry to estimate individual tree attributes in managed coniferous forests of Japan. Diameter at breast height (DBH), tree height, and stem volume were estimated by (1) TLS data only, (2) integrating TLS and UAV data with TLS tree locations, and (3) integrating TLS and UAV data with treetop detections of the tree canopy. The TLS data only approach achieved high accuracy for DBH estimations with a root mean squared error (RMSE) of 2.36 cm (RMSE% 5.6%); however, tree height was greatly underestimated, with an RMSE of 8.87 m (28.9%) and a bias of −8.39 m. Integrating TLS and UAV photogrammetric data improved tree height estimation accuracy for both the TLS tree location (RMSE of 1.89 m and a bias of −0.46 m) and the treetop detection (RMSE of 1.77 m and a bias of 0.36 m) approaches. Integrating TLS and UAV photogrammetric data also improved the accuracy of the stem volume estimations with RMSEs of 0.21 m^3 (10.8%) and 0.21 m^3 (10.5%) for the TLS tree location and treetop detection approaches, respectively. Although the tree height of suppressed trees tended to be overestimated by TLS and UAV photogrammetric data integration, a good performance was obtained for dominant trees. The results of this study indicate that the integration of TLS and UAV photogrammetry is beneficial for the accurate estimation of tree attributes in coniferous forests.

1. Introduction

Tree and forest structural attributes are essential components of forest management at various scales. Monitoring tree attributes, such as tree species, diameter at breast height (DBH), tree height, and stand volume, provides a basic understanding of forest dynamics and conditions over time (Tomppo et al., 2010). Conventionally, individual tree attributes are measured in tree-by-tree field surveys, then aggregated to obtain stand-level forest parameters based on survey objectives. Field surveys are commonly performed based on sample plots and require cost and effort to retrieve accurate tree and forest attributes. Thus, reliable, cost-effective methods to quantify tree and forest attributes are desired for operational forest management.

Forest inventories using Terrestrial Laser Scanning (TLS) have advanced in the last few decades (Liang et al., 2016). TLS collects dense point clouds using a laser scanner mounted on ground-based equipment to measure surrounding three-dimensional objects (Calders et al., 2020). Advances in TLS hardware and software have rapidly decreased the price of TLS systems, enabling more studies to investigate the utility of TLS measurements in various forest environments (Liang et al., 2016). Previous studies have attempted to estimate fundamental tree attributes, including tree height, DBH, biomass, and stem volume (e.g., (Bazezew et al., 2018; Liang et al., 2019; Wang et al., 2019; Yrttimaa et al., 2019)), and other parameters, such as tree location and stem taper (e.g., (Kelbe

* Corresponding author.
E-mail address: katsutoshimizu@ffpri.affrc.go.jp (K. Shimizu).

https://doi.org/10.1016/j.jag.2021.102658
Received 15 October 2021; Received in revised form 15 December 2021; Accepted 16 December 2021
Available online 21 December 2021

et al., 2016; Puletti et al., 2019; Pyörälä et al., 2019)). Since TLS can capture forest structures under the tree canopy, it is suitable to estimate under canopy attributes, such as DBH (Liang et al., 2018). Conversely, it is generally difficult to detect treetops and attain accurate tree height due to occlusion by understory vegetation and branches, which leads to large uncertainties and underestimations of tree height (Liang et al., 2016; Wang et al., 2019). Taller trees are particularly affected by underestimation because of the limited visibility of tree crowns (Wang et al., 2019), which hampers the accurate estimation of tree height and other structural attributes, such as stem volume.

Airborne Laser Scanning (ALS) and Unmanned Aerial Vehicle (UAV) photogrammetry are other widely used remote sensing approaches that retrieve canopy height profiles. ALS is a reliable approach for estimating accurate tree and canopy heights at a large scale (Beland et al., 2019; Puletti et al., 2020; White et al., 2016); however, it generally cannot acquire detailed structural information under the tree canopy. Thus, several studies have combined ALS and TLS measurements to retrieve tree attributes and demonstrated its estimation capabilities (Bazezew et al., 2018; Giannetti et al., 2018b; Lindberg et al., 2012). However, the extensive cost of ALS data acquisition prevents up-to-date monitoring. UAV photographs are a good alternative to regularly acquire tree and forest attribute information because of the low acquisition cost, high spatial resolution data, and flexible flight planning (Colomina and Molina, 2014; Guimarães et al., 2020). UAV-based photogrammetry can reconstruct three-dimensional forest structures as a photogrammetric point cloud through the Structure from Motion (SfM) and Multi-View Stereo (MVS) approaches (Snavely et al., 2008). Unlike point cloud data from ALS, UAV-based photogrammetry cannot provide terrain surface in forest areas (Giannetti et al., 2018a; Guimarães et al., 2020; Ota et al., 2015); however, it can capture the upper canopy layer with a comparable accuracy to ALS (Goodbody et al., 2019). The combined use of understory and terrain information from TLS and upper canopy profiles from UAV photogrammetry potentially provides complementary information for characterizing tree and forest structural attributes (Aicardi et al., 2017; FFPRI, 2020). Although this approach is promising, only limited studies have investigated its applicability for field surveys.

The estimation accuracies obtained from the integration of TLS and UAV photogrammetry can be affected by several factors, including data processing and forest stand structures. For example, the integration of the point cloud from TLS and UAV photogrammetry requires sufficient data registration. Because pulses from ALS and UAV-based laser scanning (ULS) can penetrate tree crowns, they have some overlap with the TLS point cloud, which has led to the proposal of automatic registration approaches (Polewski et al., 2019; Zhang et al., 2021). In contrast, there is little overlap between point clouds from TLS and UAV photogrammetry, especially for mature forest stands. To register these point clouds, Tian et al. (2019) investigated a tree height estimation approach that combined TLS and UAV photogrammetry based on Ground Control Points (GCPs) and registration algorithms. Although they demonstrated the applicability of this approach, the integration of TLS and UAV photogrammetry in actual forestry application is still lacking. Since the integration of TLS and UAV photogrammetry could be effective in forests with taller tree heights, further assessment of estimation accuracies in such forest environments is required. In managed plantation forests, forest stand structure varies depending largely on silvicultural treatments (e.g., thinning). As forest structure influences the estimation of tree attributes using TLS and UAV photogrammetry (Iizuka et al., 2018; Moe et al., 2020; Roşca et al., 2018; Xu et al., 2021), the investigation of estimating tree attributes and the influencing factors associated with silvicultural treatments in old managed forests would provide valuable insights for the integration of TLS and UAV photogrammetry in forest resource management. Understanding the influence of forest structure would also be useful to assess the potential use of the integration approach in other forest environments.

The objective of this study was to investigate the applicability of integrating TLS and UAV photogrammetry in the estimation of DBH, tree height, and stem volume in managed coniferous plantation forests in Japan. Specifically, we examined the accuracy of these individual tree attributes in thinned and not-thinned forests using TLS data alone and combining TLS and UAV data. When combining TLS and UAV data, we investigated two tree height estimation approaches; thus, we investigated the total of three tree height estimation approaches in this study. The thinned and not-thinned forest stands have different forest structures, thus their comparative analysis can provide insights into estimation uncertainties associated with different forest structures.

2. Study area

The study area of this research was coniferous planted forests in Yokoyama National Forest, Ibaraki prefecture, Japan (latitude 36°49′58″ N; longitude 140°35′04″ E; ~580 m above sea level) (Fig. 1). The annual rainfall in this region is about 1730 mm with a mean temperature of 10.5 °C. In the study area, Japanese cedar (*Cryptomeria Japonica*) trees were planted in 1910. Two rectangular permanent plots were established in not-thinned ("Unthin", 0.085 ha) and thinned ("Thin", 0.40 ha) forests in 1940 and 1960. The mean topographic slope was 13.9° and 9.1° in the Thin and Unthin plots, respectively, with moderate understory vegetation. All standing Japanese cedar trees were numbered and marked at breast height (i.e., 1.2 m) in both plots. In the Thin plot, thinning was undertaken at the age of 15, 30, 40, 50, and 79 years. Field surveys have been conducted about every 5–10 years since the establishment of the permanent plots.

3. Methods

3.1. Overview

In this study, we investigated three approaches for estimating the DBH, tree height, and stem volume of individual trees (Fig. 2). For each approach, DBH was obtained directly using TLS measurements, but tree height was estimated in three different ways, leading to different stem volume estimates. The approaches included: (1) using only TLS measurement data ("TLS"), (2) integrating TLS and UAV data to estimate tree height by extracting tree canopy height values just above tree locations ("TLS + UAV 1"), and (3) integrating TLS and UAV data to estimate tree height by detecting the treetops of the tree canopy ("TLS + UAV 2"). We calculated the accuracy metrics of these estimations using field survey data as a reference and then compared the accuracy of each approach.

3.2. Field survey data

We performed a field survey in two permanent plots ("Thin" and "Unthin") from 17 to 19 February 2021, at the age of 112 years (Table 1). All numbered living (Japanese cedar) trees were included in the measurements, but dead trees that were alive during the last measurement were also included. A total of 200 and 86 trees were included in the Thin and Unthin plots, respectively. DBH, tree height, and tree form class were measured for each tree during the field survey. DBH was calculated as the mean of diameter measurements obtained using steel calipers from two orthogonal directions at the marked height of 1.2 m above the ground. Tree height measurements were conducted using a Vertex IV hypsometer (Haglöf, Sweden). Tree form class was assigned based on the Terazaki's tree-form classification in the field, but later reclassified into the dominant, suppressed, and dead tree classes. We calculated the stem volume of each tree using the measured DBH and tree height in the volume equation by (Hosoda et al., 2010), which was developed by destructive measurements of trees in this region.

3.3. UAV photogrammetric data

We acquired RGB images using a DJI Phantom 4 Pro quadcopter UAV

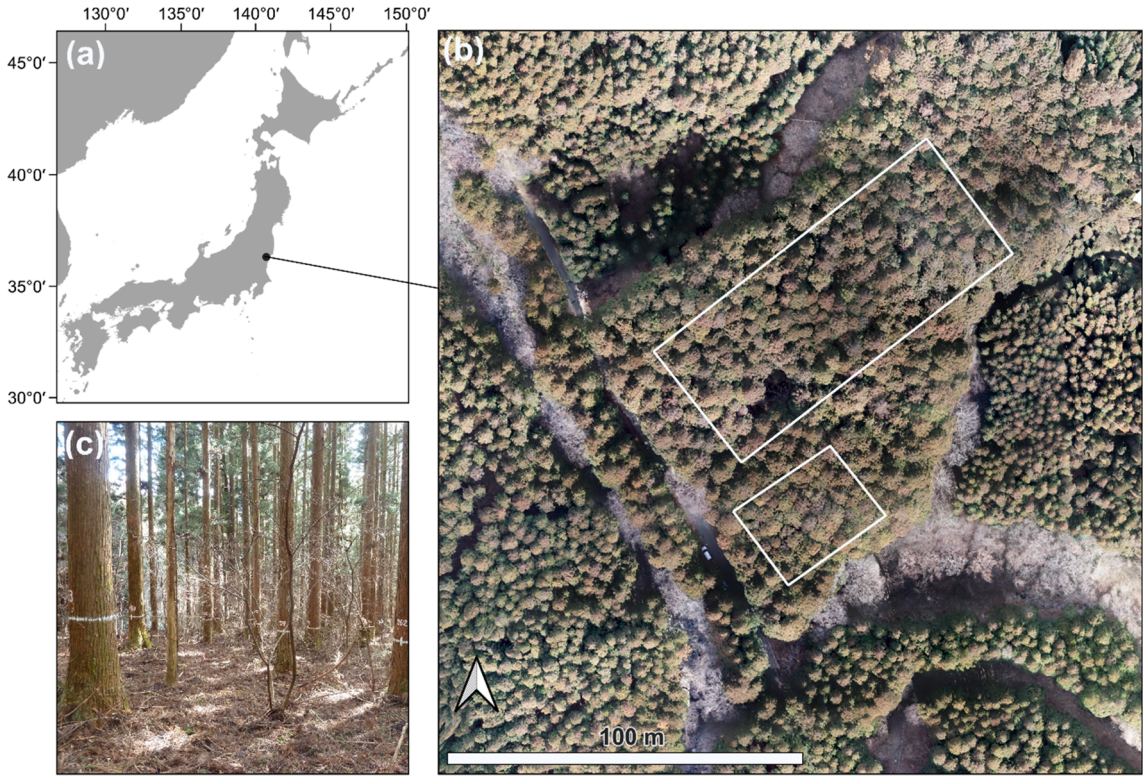

Fig. 1. The study area of this research. (a) The location of the study area in Japan. (b) Field survey plots in Thin (above) and Unthin (below) forests with an orthomosaic generated from photographs taken by the unmanned aerial vehicle (UAV). (c) Photograph of the forest stands in the Unthin plot.

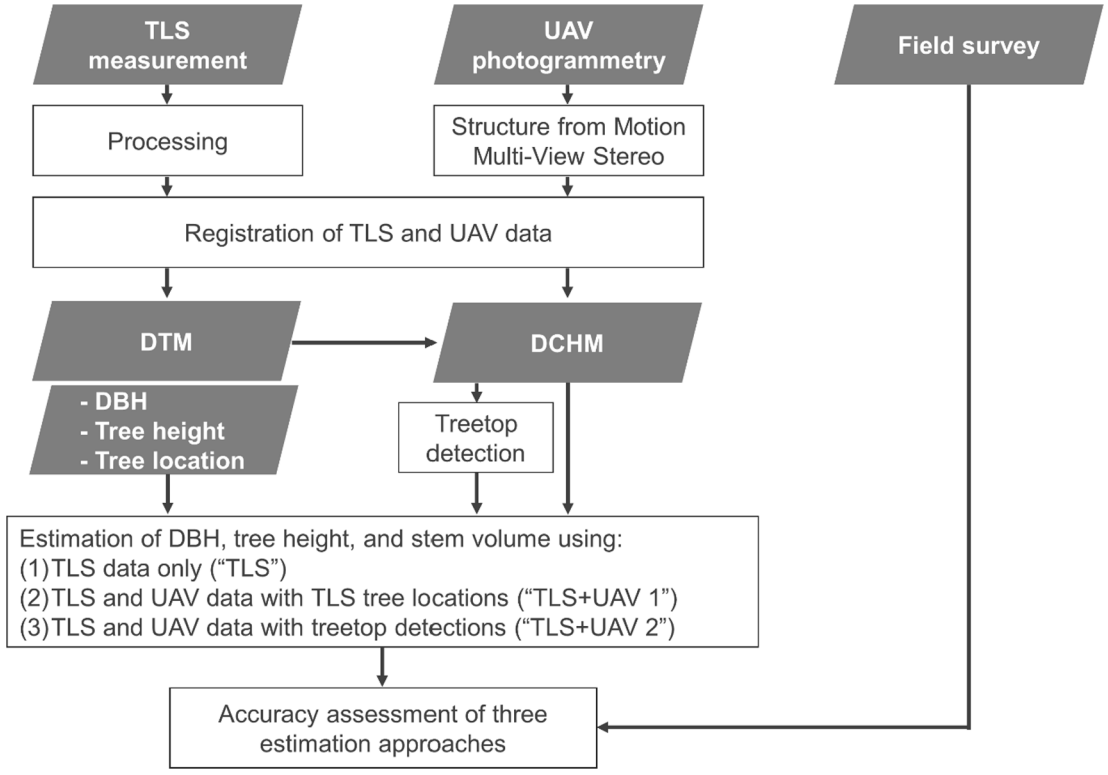

Fig. 2. Flowchart of the overall processing. Diameter at breast height (DBH), tree height, and stem volume of individual trees were estimated in three estimation approaches after the generation of a digital terrain model (DTM) from terrestrial laser scanning (TLS) and a digital canopy height model (DCHM) from UAV photogrammetric data.

Table 1
Description of measured tree attributes (DBH, tree height, and stem volume) and forest attributes in each plot in the field surveys.

	Thin	Unthin	All
Area [ha]	0.40	0.085	0.485
N of trees	200	86	286
Stand density [trees/ha]	500	1012	590
Mean DBH [cm] (min – max)	45.4 (23.8–73.4)	34.5 (21.2–56.5)	42.1 (21.2–73.4)
Mean tree height [m] (min – max)	31.7 (21.7–39.2)	28.4 (18.4–33.8)	30.7 (18.4–39.2)
Mean stem volume [m^3] (min – max)	2.28 (0.55–5.27)	1.29 (0.32–3.19)	1.98 (0.32–5.27)

(DJI, China), which had a 20-million-pixel camera, on 18 February 2021. The flight mission was controlled using the DJI GS Pro software version 2.0.14. The flight altitude was about 100 m above ground from the launched location with forward and side overlaps of 90% and 80%, respectively. The flight settings resulted in an estimated ground sampling distance of 2.7 cm. The UAV flight measurements included the entire field survey plots, covering about 6.5 ha of total area. Five GCPs were distributed within the study area. The Reach RS (Emlid, China) Global Navigation Satellite System (GNSS) receivers were used to obtain the geographical locations for each GCP. The GNSS signals were processed with a Post-Processed Kinematic solution using the RTKLIB software version 2.4.2.

Metashape Professional version 1.6.1 (Agisoft, Russia) was used to generate a photogrammetric point cloud from the photographs acquired by UAV using the SfM-MVS approach (Snavely et al., 2008). The UAV photogrammetric data was processed by image alignment, building a dense point cloud, building a mesh, and building an orthomosaic procedures. To align images and determine the internal parameters, we used a high-quality setting in Metashape Professional, resulting in a total of 162 aligned photographs. After initial image alignment, we manually identified the GCPs in corresponding photographs to optimize camera locations and orientations. In this procedure, we did not import geographical locations from the GNSS signals because the processing without GNSS locations achieved better accuracy in a preliminary analysis. Thus, the geographical locations in this analysis depended on the GNSS onboarded on the UAV. We built a dense point cloud using high-quality and mild depth filtering settings. Then, we processed the mesh building and generated an orthomosaic at 2 cm resolution. Finally, we exported the photogrammetric point cloud, which had a point density of 1973 points/m^2, for further processing.

3.4. TLS data

We implemented the TLS measurement within and around the permanent plots using the Optical Woods Ledger (OWL) (AdIn Research, Japan) on 18 February 2021. OWL is a one-legged TLS instrument equipped with the UTM-30LX-EM laser sensor (Hokuyo, Japan), offering a point density of 1.94 million points per scan (Table 2). A total of 93 scans were performed at a scanning distance of about 10 m. While scanning these locations, four scans were performed directly above the GCPs for the purpose of registering the point clouds from TLS and UAV photogrammetry in the later processing. We mapped the preliminary tree locations using the TLS data and then matched trees in the field survey and the detected trees in TLS during in situ field observations.

Table 2
Specification of OWL (sensor: UTM-30LX-EM).

Feature	Description
Pulse density	43,200 pulse/sec
Detection range	0.1–30 m
Maximum detection distance	60 m
Laser wavelength	905 nm
Measurement time per scan	45 sec
Field of view	360° (Horizontal) 270° (vertical)
Ranging accuracy	±30 mm (0.1–10 m) ±50 mm (10–30 m)
Angular Resolution	0.25°
Weight	3.7 kg

We processed the TLS point cloud using the OWL manager software version 1.7.3.1 (AdIn Research, Japan). The multi-scan TLS data were first co-registered (Tsubouchi, 2019), and then used to identify scan and tree locations and to retrieve DBH and tree height of each tree using built-in functions in the OWL manager. DBH was retrieved by fitting a circle for stem points of individual trees at breast height, whereas tree height was retrieved as the height difference between the maximum and minimum individual tree points (Muroki and I, 2019; Suematsu et al., 2020). The point cloud, scan locations, and tree locations from the TLS data had a local coordinate system. After the above processing, we eliminated trees that had an estimated tree height of < 10 m and an HD ratio (=tree height/DBH) of < 20 to remove any false detections caused by understory vegetation in the plots; however, trees that matched with the field surveyed trees were retained regardless of this filtering process. Since trees with the HD ratio of <20 are unlikely, this threshold is applicable to other forest environments, whereas the threshold for tree height (<10 m) is specific to our study area for eliminating understory vegetation. Other forest environments and study objectives would require different thresholds of tree height.

3.5. Registration of TLS and UAV data

To register the point clouds from TLS and UAV photogrammetry, two sequential steps were implemented: coarse registration using both the GCPs and scan locations and fine registration using the Iterative Closest Point (ICP) algorithm (Besl and McKay, 1992). The point cloud from TLS was transformed to match with the reference point cloud from the UAV photogrammetry in these procedures. In the coarse registration, XYZ coordinates from four GCPs that intersected with the TLS scan locations were manually extracted from the orthomosaic and the photogrammetric point cloud. Then, a transformation matrix was retrieved using the affine transformation between scan locations in the local coordinate system and the GCPs in geographic locations for the XY coordinates and the mean Z difference for the Z coordinate. The TLS tree locations and the point cloud were transformed using the retrieved transformation matrix. In the fine registration, the coarsely registered point cloud was aligned with the UAV photogrammetric point cloud using the ICP algorithm, which iteratively minimizes the distance between the points from two point sets (Besl and McKay, 1992), using CloudCompare version 2.11.3. Because TLS and UAV photogrammetry only partially shared point clouds for the same objects due to their different measurement properties, we set the overlap as 10% in the ICP algorithm. TLS tree locations were also transformed using the transformation matrix from the ICP algorithm (Fig. 3).

3.6. Generation of terrain and canopy height models

We generated a Digital Terrain Model (DTM) using the registered TLS point cloud in the R statistical software version 4.0.3 (R Core Team, 2020) with the package "lidR" (Roussel et al., 2020). A cloth simulation filtering algorithm (Zhang et al., 2016) was used to identify ground points in the TLS point cloud. The derivation of the DTM was performed by interpolating the ground points with a triangle irregular network at the spatial resolution of 0.25 m. To generate a Digital Canopy Height Model (DCHM), we first normalized the UAV photogrammetric point cloud using the DTM. The normalized photogrammetric point cloud was then used to generate a DCHM with a pit-free algorithm (Khosravipour et al., 2014) at the spatial resolution of 0.25 m. This procedure was also completed using the package "lidR".

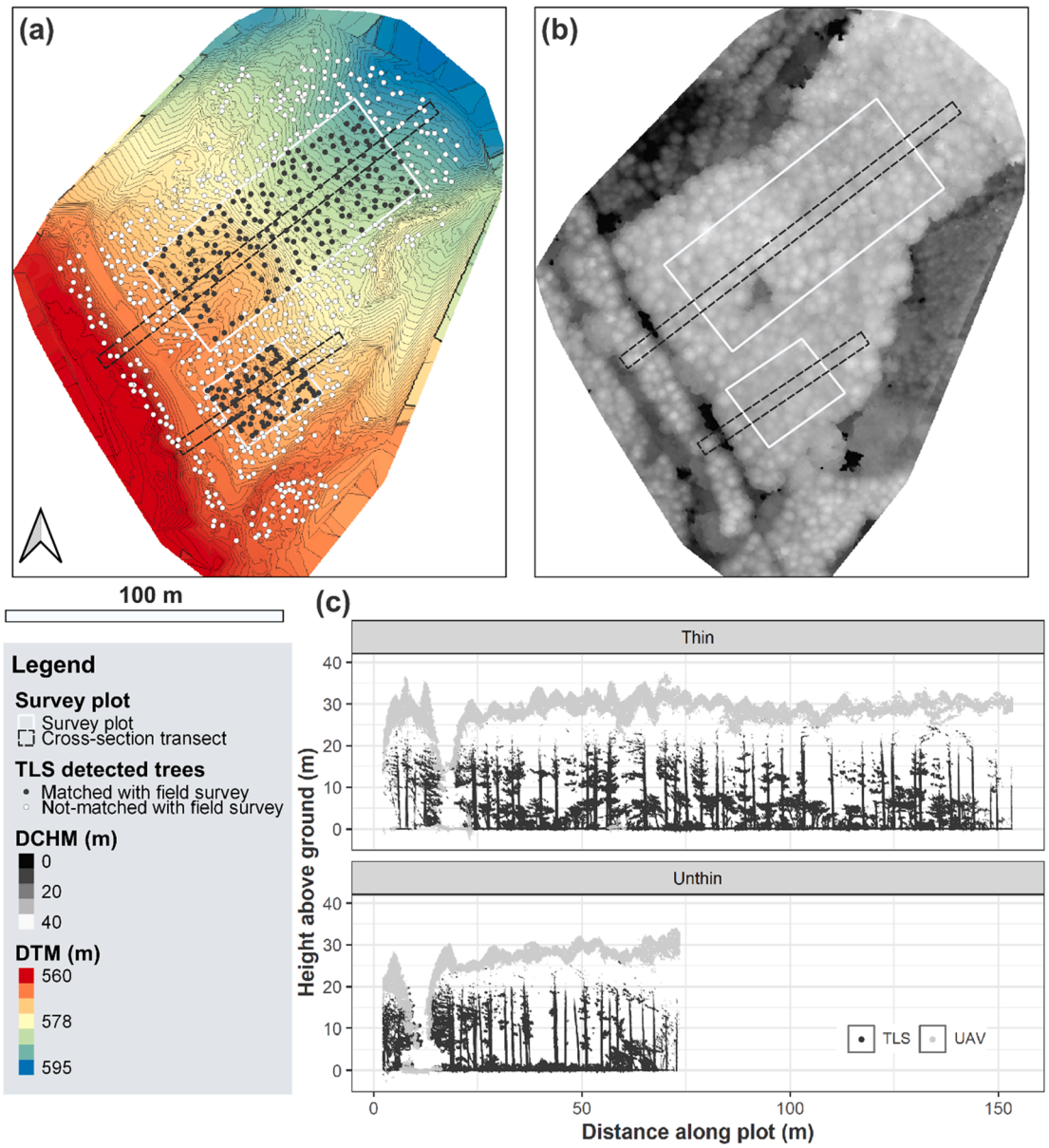

Fig. 3. The processed TLS and UAV data in the study area. (a) TLS detected tree locations with a DTM. (b) A DCHM from UAV photogrammetric data. (c) Examples of point clouds in the cross-section transects of the Thin and Unthin plots. The DTM was corrected using the signals from the Global Navigation Satellite System.

3.7. Derivation of DBH, tree height, and stem volume in each approach

We estimated tree attributes (i.e., DBH, tree height, and stem volume) using three different approaches. DBH estimation was the same for all these approaches, whereas the tree height estimation was different. Although the equation for calculating stem volume (Hosoda et al., 2010) was the same for each approach, the obtained stem volume estimates varied depending on the estimated DBH and tree height values. In this study, we investigated the following approaches: (1) tree height was directly obtained from TLS estimation ("TLS"); (2) tree height was estimated from DCHM and TLS tree locations ("TLS + UAV 1"). The DCHM values that coincided with the tree locations were treated as the tree height of individual trees in this approach; and (3) tree height was estimated through treetop detection based on DCHM and TLS tree locations ("TLS + UAV 2"). The assumption of this approach was that the treetops were not always directly above each tree's location, but rather near the corresponding tree locations. Treetop detection was performed using a local maximum filter, which was applied to the DCHM with a window size of 1.75 m and a minimum height of 10 m. The detected treetops were matched against the TLS trees based on the distance between treetops and TLS tree locations: a match was determined if a treetop and a tree location were closest to each other and within 3 m distance (Fig. 4). The matching procedure was iteratively performed for the remaining unmatched candidates until all possible candidates were matched. The DCHM values of the matched treetops were assigned as tree height. For tree locations that did not match any treetops, we assigned DCHM values directly above the tree locations as tree height.

The performance of the DBH, tree height, and stem volume estimations for individual trees in each approach was assessed using field data for the Thin, Unthin, and aggregated (All) plots. We treated the field survey as a reference for DBH and tree height. For stem volume, we used the calculated value from the volume equation as a reference. We calculated the Root Mean Squared Error (RMSE), Mean Absolute Error (MAE), bias, coefficient of determination (R^2), and Concordance Correlation Coefficient (CCC) (Lin, 1989) for the trees that matched with the field survey data. For RMSE, MAE, and bias, we also calculated the metrics normalized by the mean values of the field survey (RMSE%, MAE%, and bias%). The RMSE, MAE, bias, R^2, and CCC were calculated

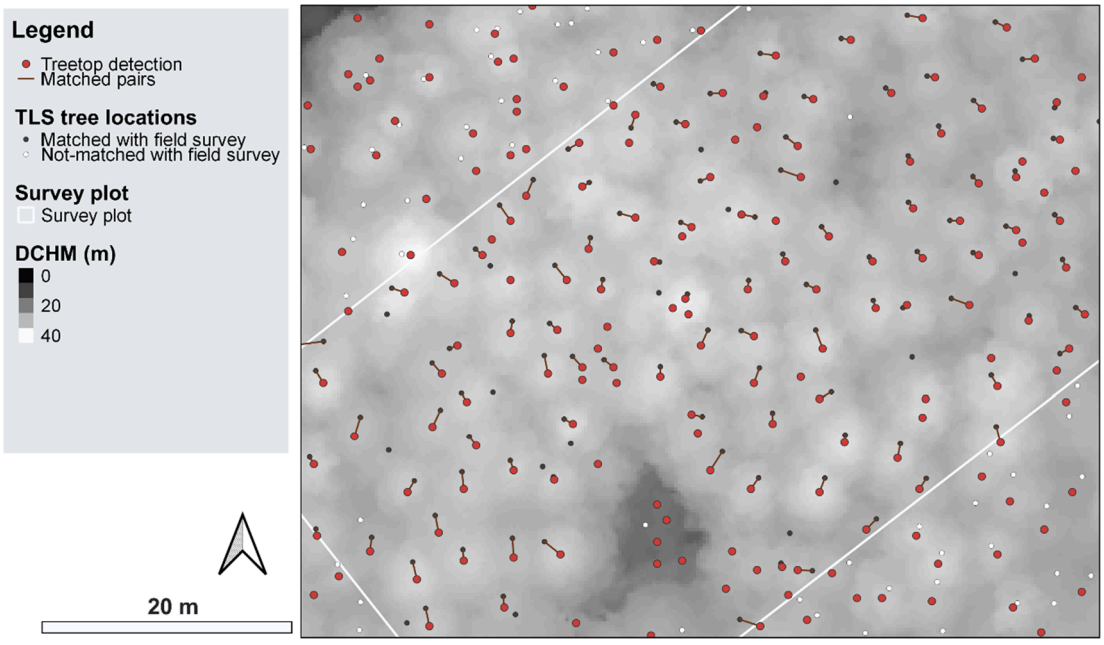

Fig. 4. Example of the matching results of TLS tree locations and treetop detection in the Thin plot. Matching results are shown only for the TLS detected trees within the plot.

as follows:

$$RMSE = \sqrt{\frac{1}{n}\sum_{i=1}^{n}(x_i - y_i)^2} \quad (1)$$

$$MAE = \frac{1}{n}\sum_{i=1}^{n}|x_i - y_i| \quad (2)$$

$$bias = \frac{1}{n}\sum_{i=1}^{n}(x_i - y_i) \quad (3)$$

$$R^2 = 1 - \frac{\sum_{i=1}^{n}(y_i - x_i)^2}{\sum_{i=1}^{n}(y_i - \bar{y})^2} \quad (4)$$

$$CCC = \frac{2\sigma_{xy}}{\sigma_x^2 + \sigma_y^2 + (\bar{x} - \bar{y})^2} \quad (5)$$

where, n is the number of trees that matched with the field survey; x_i is the estimated value of tree i in each approach; y_i is the measured value of tree i in the field survey; $\bar{x}$ is the mean estimated value in each approach; $\bar{y}$ is the mean value of field survey; σ_{xy} is the covariance for the estimated and measured values in each approach; σ_x is the variance of the estimated values in each approach; and σ_y is the variance of the measured values in the field survey.

4. Results

4.1. TLS tree detection

TLS measurement detected 208 and 107 trees in the Thin and Unthin plots, respectively (Table 3). Although all of the field surveyed trees were detected in both the Thin and Unthin plots, false tree detection (i.e., trees detected in TLS but not measured in field survey) was observed for both plots, with 8 and 21 trees in the Thin and Unthin plots, leading to the ratio of correct TLS detection of 96.2% (=200/208) and 80.4% (=86/107), respectively. In the Thin plot, five of these trees were dead trees, two were overestimated trees, and the other was a broadleaf tree, whereas all 21 trees were confirmed as dead trees in the Unthin plot. The ratio of correct TLS detection was lower in the Unthin plot than in the Thin plot, indicating that false tree detection occurred more frequently in the Unthin plot.

Table 3
Results of TLS tree detection and matching with the field surveys.

	Thin	Unthin	All
N of trees in field survey	200	86	286
N of trees in TLS detection	208	107	315
N of TLS trees matched with field survey	200	86	286
N of TLS trees not-matched with field survey	8	21	29
Ratio of correct field tree detection	100%	100%	100%
Ratio of correct TLS detection	96.2%	80.4%	90.8%

4.2. DBH estimation by TLS

The comparison of field measured DBH with TLS measured DBH is shown in Fig. 5. The RMSEs of the DBH estimations were 2.27 cm (RMSE %: 5.0%), 2.54 cm (7.4%), and 2.36 cm (5.6%) for Thin, Unthin, and All plots, respectively (Table 4). All accuracy metrics achieved a better performance in the Thin plot compared to those in the Unthin plot. The estimations were positively biased, especially in the Unthin plot (1.16 cm, 3.4%). The CCCs were larger than 0.94 in all three patterns.

4.3. Tree height estimation in each approach

The tree height estimations from each approach are compared to reference field survey data in Fig. 6. Tree height was largely underestimated by the "TLS" approach (bias of −8.39 m for All plot; Table 5). The RMSE (8.87 m), MAE (8.40 m), R^2 (0.186), and CCC (0.071) obtained from the "TLS" approach also revealed lower accuracies compared to other approaches. In contrast, bias and the other accuracy metrics were improved when combined with the UAV data. The RMSE/MAE of all combined plots were 1.89 m (6.2%)/1.38 m (4.5%) and 1.77 m (5.7%)/1.14 m (3.7%) for the "TLS + UAV 1" and "TLS + UAV 2" approaches, respectively. The "TLS + UAV 2" generally achieved better performance than the "TLS + UAV 1" approach; however, in the Unthin plot, RMSE and bias were better using the "TLS + UAV 1" approach. The bias of the tree height estimation in "TLS + UAV 1" was slightly negative in the Thin and All plots, whereas the estimation in "TLS + UAV 2" approach was positively biased in the all plots. In the "TLS" approach,

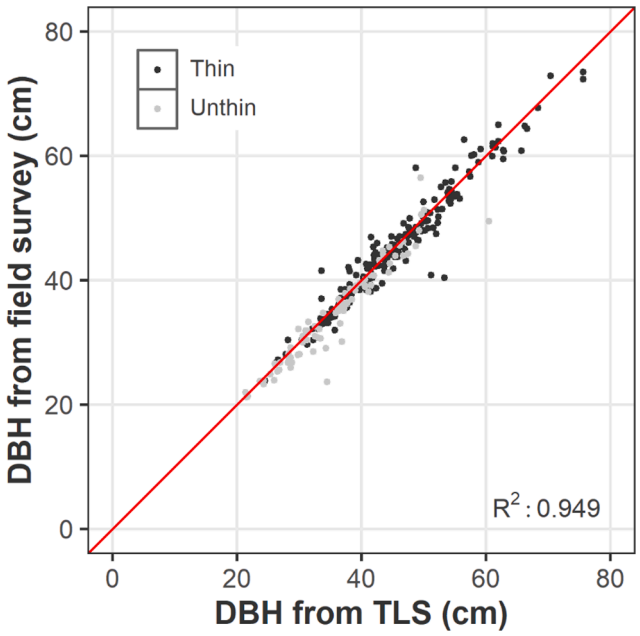

Fig. 5. Comparison of diameter at breast height (DBH) of individual trees using the TLS measurements and field surveys.

Table 4
Accuracies of DBH estimation using TLS. The metrics normalized by the mean field survey values are shown in parentheses.

Plot	RMSE [cm]	MAE [cm]	bias [cm]	R^2	CCC
Thin	2.27 (5.0%)	1.51 (3.3%)	0.38 (0.8%)	0.940	0.969
Unthin	2.54 (7.4%)	1.65 (4.8%)	1.16 (3.4%)	0.916	0.946
All	2.36 (5.6%)	1.55 (3.7%)	0.62 (1.5%)	0.949	0.972

one tree had a tree height of 0 m, which was confirmed to be a forked tree.

In the treetop detection of the "TLS + UAV 2" approach, 78.3% of the TLS trees were detected in the local maximum filter procedure. The RMSE of the detected trees (1.51 m, 4.8%) was lower than that of the undetected trees (2.48 m, 8.7%), which were estimated using the DCHM values directly above the tree locations. The biases of the detected and undetected trees were 0.34 m and 0.42 m, respectively.

The tree height of each tree class revealed that suppressed and dead trees were likely to be underestimated in the "TLS + UAV 1" and "TLS + UAV 2" approaches (Fig. 7). Although the dominant class occupied 95.1% of all trees and relatively few trees were assigned to the suppressed and dead classes, overestimation was observed in both classes. The bias of suppressed and dead tree classes were 4.18 m and 6.54 m, respectively, for the "TLS + UAV 1" approach, and 4.95 m and 6.74 m, respectively, for the "TLS + UAV 2" approach.

4.4. Stem volume estimation in each approach

The tree height estimates affected the accuracy of the stem volume estimation in this study (Fig. 8). Overall, the approaches that integrated both TLS and UAV photogrammetry achieved higher accuracies and lower biases (Table 6). The best accuracy metrics for the All plot were obtained using the "TLS + UAV 2" approach for RMSE (0.21 m^3), MAE (0.14 m^3), R^2 (0.954), and CCC (0.975) with slightly lower values for the "TLS + UAV 1" (RMSE, MAE, R^2, and CCC of 0.21 m^3, 0.14 m^3, 0.950, and 0.972, respectively). The bias was more improved in "TLS + UAV 1" than in "TLS + UAV 2".

5. Discussion

TLS is a promising technology for estimating under canopy tree attributes, such as DBH; however, previous studies have indicated that tree height is often underestimated using TLS data (Wang et al., 2019). This could be problematic when estimating tree attributes in old

Table 5
Accuracies of tree height estimation for each approach. The metrics normalized by the mean field survey values are shown in parentheses.

Approach	Plot	RMSE [m]	MAE [m]	bias [m]	R^2	CCC
TLS	Thin	9.16 (28.9%)	8.80 (27.7%)	−8.80 (−27.7%)	0.062	0.024
	Unthin	8.17 (28.8%)	7.47 (26.3%)	−7.45 (−26.2%)	0.127	0.085
	All	8.87 (28.9%)	8.40 (27.3%)	−8.39 (−27.3%)	0.186	0.071
TLS + UAV 1	Thin	1.64 (5.2%)	1.22 (3.9%)	−0.77 (−2.4%)	0.631	0.738
	Unthin	2.39 (8.4%)	1.74 (6.1%)	0.27 (1.0%)	0.325	0.450
	All	1.89 (6.2%)	1.38 (4.5%)	−0.46 (−1.5%)	0.617	0.733
TLS + UAV 2	Thin	1.41 (4.4%)	0.95 (3.0%)	0.17 (0.5%)	0.658	0.804
	Unthin	2.40 (8.5%)	1.58 (5.6%)	0.81 (2.8%)	0.387	0.499
	All	1.77 (5.7%)	1.14 (3.7%)	0.36 (1.2%)	0.658	0.782

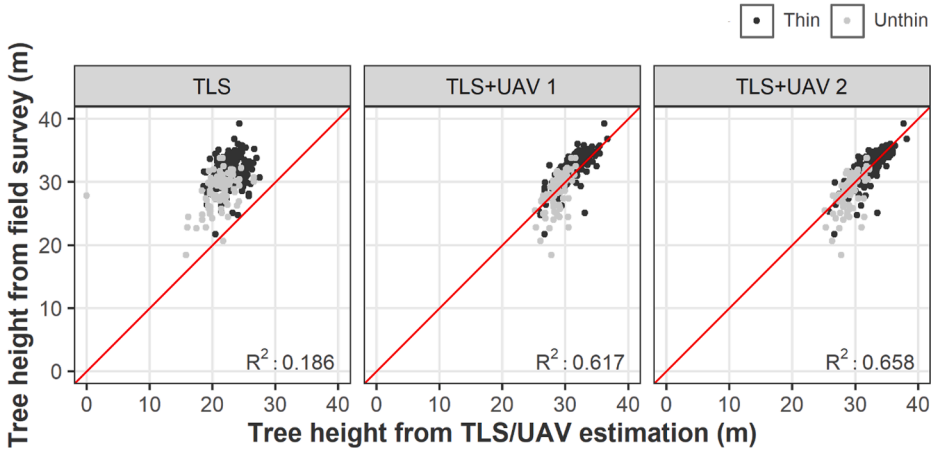

Fig. 6. Comparison of tree height estimations from "TLS", "TLS + UAV 1", and "TLS + UAV 2" approaches against the field survey measurements.

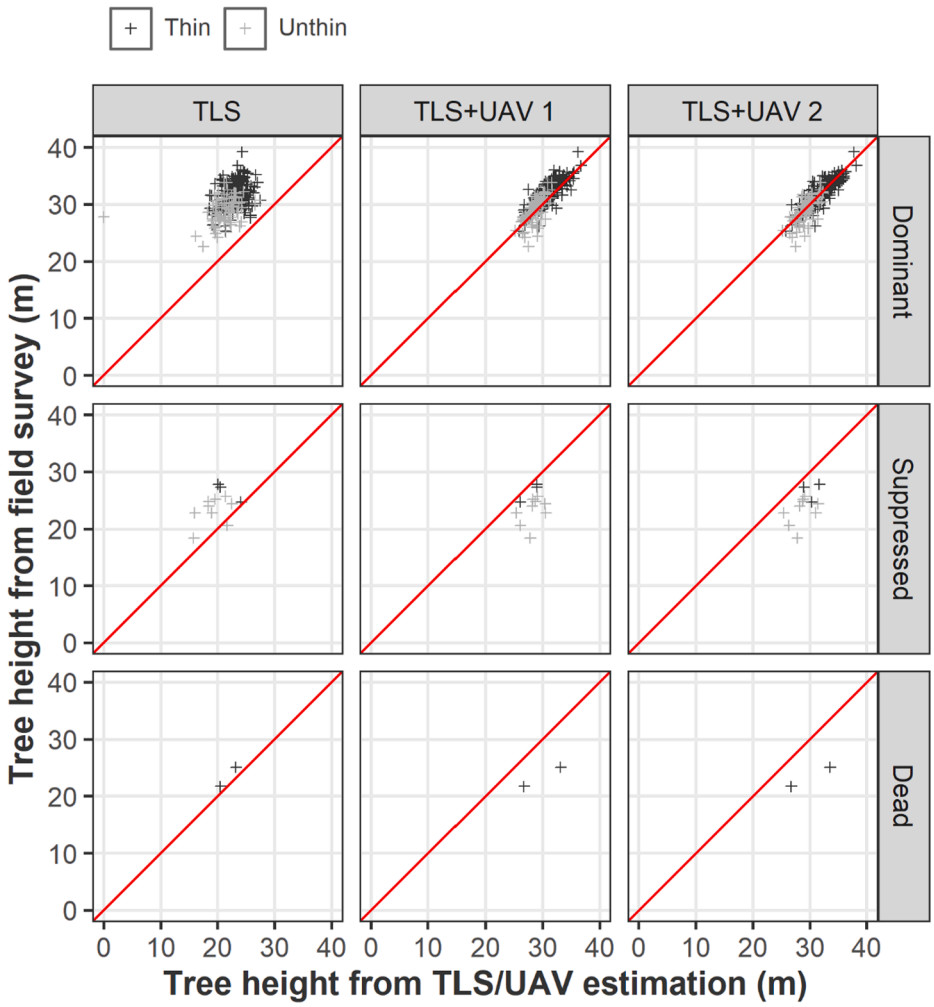

Fig. 7. Comparison of tree height estimations of the dominant, suppressed, and dead tree classes in the "TLS", "TLS + UAV 1", and "TLS + UAV 2" approaches against the field survey measurements.

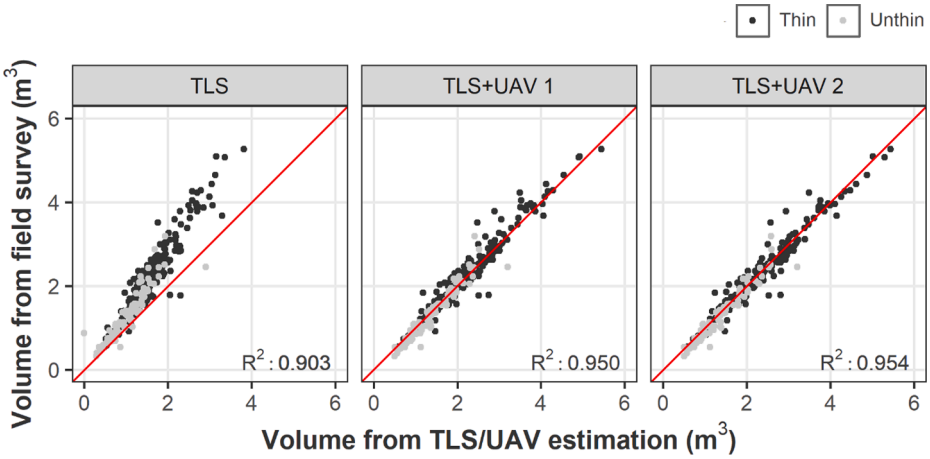

Fig. 8. Comparison of stem volume estimation of "TLS", "TLS + UAV 1", and "TLS + UAV 2" approaches against the field survey measurements.

managed forests with taller tree canopies. In this study, we investigated the integration of TLS and UAV photogrammetric data to estimate DBH, tree height, and stem volume in managed conifer plantations in Japan. The results indicated the promising prospect of integrating TLS and UAV data for the accurate estimation of individual tree attributes.

All field surveyed trees were successfully detected by the TLS measurements in both Thin and Unthin plots. Tree detection in multi-scan TLS is influenced by forest structures and scanning setups (Liang et al., 2016). Higher stand density and trees with smaller DBH generally decrease tree detection (Gollob et al., 2019). In this study, stand density was not high (500 and 1012 trees/ha) and all trees had DBH values that were larger than 20 cm, which possibly led to the high detection

Table 6
Accuracies of stem volume estimation for each approach. The metrics normalized by the mean field survey values are shown in parentheses.

Approach	Plot	RMSE [m^3]	MAE [m^3]	bias [m^3]	R^2	CCC
TLS	Thin	0.76 (33.2%)	0.66 (28.7%)	−0.65 (−28.3%)	0.891	0.632
	Unthin	0.39 (30.5%)	0.30 (23.7%)	−0.28 (−21.9%)	0.824	0.766
	All	0.67 (33.7%)	0.55 (27.8%)	−0.54 (−27.1%)	0.903	0.712
TLS + UAV 1	Thin	0.22 (9.8%)	0.15 (6.5%)	−0.04 (−1.8%)	0.940	0.967
	Unthin	0.19 (14.7%)	0.13 (10.2%)	0.06 (4.5%)	0.916	0.947
	All	0.21 (10.8%)	0.14 (7.2%)	−0.01 (−0.5%)	0.950	0.972
TLS + UAV 2	Thin	0.22 (9.5%)	0.15 (6.5%)	0.03 (1.5%)	0.944	0.971
	Unthin	0.19 (14.6%)	0.14 (10.7%)	0.09 (6.7%)	0.925	0.950
	All	0.21 (10.5%)	0.14 (7.3%)	0.05 (2.5%)	0.954	0.975

accuracy. In addition, the scanning distance of about 10 m was enough to detect all trees. Suematsu et al. (2020) showed that scanning distances longer than 10 m using OWL would decrease detection accuracy, especially in forests with understory vegetation. This was not the case for our study, even with moderate understory vegetation. False detection trees were mostly caused by dead trees in this study. Because there existed standing dead trees in forests, it was reasonable to include them in the TLS measurements; however, dead trees are usually not suitable for timber extraction, and forest resources would be overestimated if dead trees are treated as exploitable trees. Although there are few studies that have examined an automatic method for identifying dead trees using TLS data (Marchi et al., 2018), automated procedures are required for operational forest monitoring.

As expected, the DBH estimations using the TLS data achieved high accuracy with an RMSE of 2.36 cm (5.6%) and a CCC of 0.972 for the All plot. This result is comparable with the estimation accuracy reported in previous studies, with RMSEs of 1.1–3.8 cm (5.4–13.1%), using multi-scan TLS measurements in different forest environments (Bazezew et al., 2018; Giannetti et al., 2018b; Gollob et al., 2019; Lindberg et al., 2012; Liu et al., 2018; Maas et al., 2008). Similar findings were obtained by previous studies focused on the coniferous plantation forests in Japan, with an RMSE of 1.1 cm (4.5%) (Suematsu et al., 2020) and MAEs of 2.2–3.9% (Nishizono et al., 2020) and 3.0–4.6% (Kitahara et al., 2020) for Japanese cypress (*Chamaecyparis obtusa*) forests, and RMSEs of 1.1–1.3 cm (Matsumura et al., 2020) and 3.2 cm (Muroki and I, 2019) for Japanese cedar forests using the OWL measurements. The accuracies in the Thin plot generally had a better performance than those in the Unthin plot. The accuracies of DBH estimations are largely affected by forest structures (Liang et al., 2018). Thus, the high stand density in the Unthin plot might have decreased the point clouds on the stems, leading to lower estimation accuracies in this study.

The tree height estimation using only the TLS data showed a large underestimation with the biases of −8.80 m and −7.45 m for the Thin and Unthin plots, respectively. The underestimation of taller trees has also been observed in previous studies (e.g., (Liang et al., 2018; Wang et al., 2019)), mainly due to occlusions caused by trees and understory vegetation. In this study, mean tree height was relatively high (i.e., 30.7 m) compared to the detection range of TLS (i.e., 0.1–30 m). The capacity of the TLS laser sensor made it difficult to detect the treetops using the TLS data, as obviously shown in the example point cloud in Fig. 3. Although the underestimation of tree height was severe in this study, the underestimations of tree height were also found in previous studies using other TLS sensors (e.g., (Matsumura et al., 2020; Wang et al., 2019)). The integration of the UAV photogrammetric data greatly improved the estimation biases and accuracies in both the Thin and Unthin plots. This is not surprising because tree height from the UAV-SfM approach can, in case a valid DTM is available, provide accurate estimates (Goodbody et al., 2019; Iglhaut et al., 2019; Puliti et al., 2019; Vaglio Laurin et al., 2019). Tree height estimation with treetop detection ("TLS + UAV 2") generally showed higher accuracies (RMSE: 1.77 m, 5.7%) compared to the tree height estimation based on tree location ("TLS + UAV 1") (RMSE: 1.89 m, 6.2%), revealing that the treetops were not always directly above tree locations and should be detected for accurate estimation. In contrast, some smaller trees, especially for the suppressed trees, showed an overestimation of tree height (Fig. 7). Because we used DCHM values to estimate tree height, trees occluded by other taller trees can have overestimated tree height. Relatively larger overestimations in the Unthin plot, which had smaller tree heights than the Thin plot, can be partially explained by this reason. A more sophisticated approach for detecting suppressed trees might improve the accuracy of tree height estimations. In addition, although the treetop detection approach ("TLS + UAV 2") achieved high accuracies in Japanese cedar forests in this study, the "TLS + UAV 1" approach might be more suited to forests with treetops that are difficult to detect using the local maximum filter due to species-specific crown forms (e.g., Japanese cypress, Japanese larch, and broadleaf species). Another possible solution to estimate the accurate tree height of individual trees in such forests would be using TLS point clouds for characterizing stem taper and deriving the potential treetops. This should be investigated in future studies.

Stem volume was underestimated by the "TLS" approach due to the underestimation of tree height. Integrating UAV photogrammetry achieved better accuracies in both the Thin and Unthin plots. Although "TLS + UAV 2" achieved higher accuracies in tree height estimation, both "TLS + UAV 1" and "TLS + UAV 2" showed similar accuracies for the stem volume estimations. The integration of TLS data and other data sources for estimating stem volume and other tree attributes have been previously investigated in several studies, especially in combination with ALS (e.g., (Bazezew et al., 2018; Giannetti et al., 2018b; Lindberg et al., 2012)). These studies showed improved accuracies mainly for tree height estimations by integrating multiple data sources. This study revealed that the integration of TLS and UAV photogrammetric data also improved the estimation accuracies of tree height and stem volume.

Although it is quite difficult to confirm which data source should be used for the integration, the integration of TLS and UAV photogrammetric data can be used as an alternative approach in forests with suitable conditions. As UAV photogrammetry can only acquire the upper tree canopy surface, the overestimation of tree height would deteriorate in multi-layer forests with many suppressed trees that are not visible from photographs. In addition, the registration in this study required TLS scans on GCPs, which might be difficult to obtain for forest stands with dense canopy cover. Although coarse registration approaches without GCPs have been recently proposed (e.g., Hyyppä et al., 2021), the applicability of those approaches is still unclear in our study area. Furthermore, since the TLS point cloud mainly captures the under canopy and UAV photogrammetric point cloud mainly captures the upper canopy structure, they shared only a portion of points. For this reason, the ICP algorithm in the registration process might not be applicable to forests with few gaps or roads. In such forest environments, the integration of TLS and UAV photogrammetry should be cautiously used. In addition, TLS measurements might not be feasible in dense understory vegetation due to occlusion effects (Kelbe et al., 2016; Tremblay and Béland, 2018), even if the UAV flight was successfully completed. More investigations in additional forest conditions are required to better understand the integration of TLS and UAV photogrammetry.

The derivation of stem volume from point clouds has the potential to improve estimation accuracy, as demonstrated by previous studies (Calders et al., 2015; Liang et al., 2016). However, the TLS point cloud in this study did not reach the upper canopy, and thus it might decrease

estimation accuracy even with sophisticated algorithms. In such a case, the integration of UAV-based laser scanning (ULS) might provide complementary data thanks to the dense point clouds obtained from ULS (Liang et al., 2019; Polewski et al., 2019). Although ULS is a promising technology, it still requires investigation into its usage in various forest environments. The cost and spatial coverage are also important aspects for operational forest monitoring. The integration of TLS and UAV photogrammetry should also be compared to such remote sensing technology to investigate cost-effective monitoring approaches.

6. Conclusion

This study examined the integration of TLS and UAV photogrammetric data to estimate DBH, tree height, and stem volume in thinned and not-thinned plots in coniferous planted forests in Japan. We evaluated the accuracies of estimation approaches using TLS data alone and integrating TLS and UAV data. As expected, DBH estimation using TLS data achieved high accuracies, whereas tree height estimation revealed a large underestimation when using TLS data alone. In contrast, the integration of TLS and UAV photogrammetric data greatly improved the tree height estimation accuracies. In particular, tree height estimation achieved improved accuracies by extracting the DCHM values at the treetops as detected with a local maximum filter. The accuracy of the stem volume estimations was also improved by integrating the TLS and UAV photogrammetry, which was mainly due to the improved tree height estimations. Although the approach presented here might result in low estimation accuracies in multi-layer forests and requires some specific conditions for the registration process, it is still useful to accurately estimate the DBH, tree height, and stem volume of individual trees, especially in coniferous planted forests with taller trees. The integration of TLS and UAV photogrammetry could be used for estimating accurate and up-to-date tree attributes in forest inventory, improving yield prediction, and understanding forest dynamics of coniferous forests, potentially in other study regions. Future studies should investigate the cost-efficient and operational use of TLS and UAV photogrammetry in actual forest management both in coniferous and broadleaved forests.

Funding

This work was supported by Grant-in-Aid for Forestry Promotion from Japan Forest Foundation. The funding body played no role in this study.

CRediT authorship contribution statement

Katsuto Shimizu: Software, Methodology, Validation, Formal analysis, Investigation, Data curation, Writing – original draft, Visualization. **Tomohiro Nishizono:** Conceptualization, Methodology, Software, Formal analysis, Investigation, Data curation, Writing – review & editing, Supervision, Funding acquisition. **Fumiaki Kitahara:** Conceptualization, Methodology, Software, Formal analysis, Investigation, Data curation, Writing – review & editing, Funding acquisition. **Keiko Fukumoto:** Investigation, Writing – review & editing. **Hideki Saito:** Methodology, Writing – review & editing.

Declaration of Competing Interest

The authors declare that they have no known competing financial interests or personal relationships that could have appeared to influence the work reported in this paper.

Acknowledgments

We thank the editor and two anonymous reviewers for their constructive comments.

Data availability

The data supporting this article will be shared from the corresponding author upon reasonable request.

References

Aicardi, I., Dabove, P., Lingua, A.M., Piras, M., 2017. Integration between TLS and UAV photogrammetry techniques for forestry applications. IForest 10, 41–47. https://doi.org/10.3832/ifor1780-009.

Bazezew, M.N., Hussin, Y.A., Kloosterman, E.H., 2018. Integrating Airborne LiDAR and Terrestrial Laser Scanner forest parameters for accurate above-ground biomass/carbon estimation in Ayer Hitam tropical forest, Malaysia. Int. J. Appl. Earth Obs. Geoinf. 73, 638–652. https://doi.org/10.1016/J.JAG.2018.07.026.

Beland, M., Parker, G., Sparrow, B., Harding, D., Chasmer, L., Phinn, S., Antonarakis, A., Strahler, A., 2019. On promoting the use of lidar systems in forest ecosystem research. For. Ecol. Manage. 450, 117484. https://doi.org/10.1016/j.foreco.2019.117484.

Besl, P.J., McKay, N.D., 1992. A Method for Registration of 3-D Shapes. IEEE Trans. Pattern Anal. Mach. Intell. 14 (2), 239–256. https://doi.org/10.1109/34.121791.

Calders, K., Adams, J., Armston, J., Bartholomeus, H., Bauwens, S., Bentley, L.P., Chave, J., Danson, F.M., Demol, M., Disney, M., Gaulton, R., Krishna Moorthy, S.M., Levick, S.R., Saarinen, N., Schaaf, C., Stovall, A., Terryn, L., Wilkes, P., Verbeeck, H., 2020. Terrestrial laser scanning in forest ecology: Expanding the horizon. Remote Sens. Environ. 251, 112102. https://doi.org/10.1016/j.rse.2020.112102.

Calders, K., Newnham, G., Burt, A., Murphy, S., Raumonen, P., Herold, M., Culvenor, D., Avitabile, V., Disney, M., Armston, J., Kaasalainen, M., McMahon, S., 2015. Nondestructive estimates of above-ground biomass using terrestrial laser scanning. Methods Ecol. Evol. 6 (2), 198–208. https://doi.org/10.1111/2041-210X.12301.

Colomina, I., Molina, P., 2014. Unmanned aerial systems for photogrammetry and remote sensing: A review. ISPRS J. Photogramm. Remote Sens. 92, 79–97. https://doi.org/10.1016/j.isprsjprs.2014.02.013.

FFPRI, 2020. Novel forest inventory using Terrestrial Laser Scanning and Unmanned Aerial Vehicle (in Japanese).

Giannetti, F., Chirici, G., Gobakken, T., Næsset, E., Travaglini, D., Puliti, S., 2018a. A new approach with DTM-independent metrics for forest growing stock prediction using UAV photogrammetric data. Remote Sens. Environ. 213, 195–205. https://doi.org/10.1016/J.RSE.2018.05.016.

Giannetti, F., Puletti, N., Quatrini, V., Travaglini, D., Bottalico, F., Corona, P., Chirici, G., 2018b. Integrating terrestrial and airborne laser scanning for the assessment of single-tree attributes in Mediterranean forest stands. Eur. J. Remote Sens. 51 (1), 795–807. https://doi.org/10.1080/22797254.2018.1482733.

Gollob, C., Ritter, T., Wassermann, C., Nothdurft, A., 2019. Influence of Scanner Position and Plot Size on the Accuracy of Tree Detection and Diameter Estimation Using Terrestrial Laser Scanning on Forest Inventory Plots. Remote Sens. 11, 1602. https://doi.org/10.3390/rs11131602.

Goodbody, T.R.H., Coops, N.C., White, J.C., 2019. Digital Aerial Photogrammetry for Updating Area-Based Forest Inventories: A Review of Opportunities, Challenges, and Future Directions. Curr. For. Reports 5 (2), 55–75. https://doi.org/10.1007/s40725-019-00087-2.

Guimarães, N., Pádua, L., Marques, P., Silva, N., Peres, E., Sousa, J.J., 2020. Forestry Remote Sensing from Unmanned Aerial Vehicles: A Review Focusing on the Data, Processing and Potentialities. Remote Sens. 12, 1046. https://doi.org/10.3390/rs12061046.

Hosoda, K., Mitsuda, Y., Iehara, T., 2010. Differences between the present stem volume tables and the values of the volume equations, and their correction. Japanese J. For. Plan. 44, 23–39. https://doi.org/10.20659/jjfp.44.2_23.

Hyyppä, E., Muhojoki, J., Yu, X., Kukko, A., Kaartinen, H., Hyyppä, J., 2021. Efficient coarse registration method using translation- and rotation-invariant local descriptors towards fully automated forest inventory. ISPRS Open J. Photogramm. Remote Sens. 2, 100007. https://doi.org/10.1016/j.ophoto.2021.100007.

Iglhaut, J., Cabo, C., Puliti, S., Piermattei, L., O'Connor, J., Rosette, J., 2019. Structure from Motion Photogrammetry in Forestry: a Review. Curr. For. Reports 5 (3), 155–168. https://doi.org/10.1007/s40725-019-00094-3.

Iizuka, K., Yonehara, T., Itoh, M., Kosugi, Y., 2018. Estimating Tree Height and Diameter at Breast Height (DBH) from Digital Surface Models and Orthophotos Obtained with an Unmanned Aerial System for a Japanese Cypress (Chamaecyparis obtusa) Forest. Remote Sens. 10, 13. https://doi.org/10.3390/RS10010013.

Kelbe, D., van Aardt, J., Romanczyk, P., van Leeuwen, M., Cawse-Nicholson, K., 2016. Marker-Free Registration of Forest Terrestrial Laser Scanner Data Pairs with Embedded Confidence Metrics. IEEE Trans. Geosci. Remote Sens. 54 (7), 4314–4330. https://doi.org/10.1109/TGRS.2016.2539219.

Khosravipour, A., Skidmore, A.K., Isenburg, M., Wang, T., Hussin, Y.A., 2014. Generating Pit-free Canopy Height Models from Airborne Lidar. Photogramm. Eng. Remote Sens. 80 (9), 863–872. https://doi.org/10.14358/PERS.80.9.863.

Kitahara, F., Nishizono, T., Hosoda, K., Kodani, E., 2020. Comparison of forest measurement errors using two types of terrestrial laser scanning. Japanese J. For. Plan. 54, 63–66. https://doi.org/10.20659/jjfp.54.1_63.

Liang, X., Hyyppä, J., Kaartinen, H., Lehtomäki, M., Pyörälä, J., Pfeifer, N., Holopainen, M., Brolly, G., Francesco, P., Hackenberg, J., Huang, H., Jo, H.-W., Katoh, M., Liu, L., Mokroš, M., Morel, J., Olofsson, K., Poveda-Lopez, J., Trochta, J., Wang, D., Wang, J., Xi, Z., Yang, B., Zheng, G., Kankare, V., Luoma, V., Yu, X., Chen, L., Vastaranta, M., Saarinen, N., Wang, Y., 2018. International benchmarking

of terrestrial laser scanning approaches for forest inventories. ISPRS J. Photogramm. Remote Sens. 144, 137–179. https://doi.org/10.1016/J.ISPRSJPRS.2018.06.021.
Liang, X., Kankare, V., Hyyppä, J., Wang, Y., Kukko, A., Haggrén, H., Yu, X., Kaartinen, H., Jaakkola, A., Guan, F., Holopainen, M., Vastaranta, M., 2016. Terrestrial laser scanning in forest inventories. ISPRS J. Photogramm. Remote Sens. 115, 63–77. https://doi.org/10.1016/J.ISPRSJPRS.2016.01.006.
Liang, X., Wang, Y., Pyörälä, J., Lehtomäki, M., Yu, X., Kaartinen, H., Kukko, A., Honkavaara, E., Issaoui, A.E.I., Nevalainen, O., Vaaja, M., Virtanen, J.-P., Katoh, M., Deng, S., 2019. Forest in situ observations using unmanned aerial vehicle as an alternative of terrestrial measurements. For. Ecosyst. 6, 20. https://doi.org/10.1186/s40663-019-0173-3.
Lin, L.-K., 1989. A Concordance Correlation Coefficient to Evaluate Reproducibility. Biometrics 45 (1), 255. https://doi.org/10.2307/2532051.
Lindberg, E., Holmgren, J., Olofsson, K., Olsson, H., 2012. Estimation of stem attributes using a combination of terrestrial and airborne laser scanning. Eur. J. For. Res. 131 (6), 1917–1931. https://doi.org/10.1007/s10342-012-0642-5.
Liu, G., Wang, J., Dong, P., Chen, Y., Liu, Z., 2018. Estimating Individual Tree Height and Diameter at Breast Height (DBH) from Terrestrial Laser Scanning (TLS) Data at Plot Level. Forests 9, 398. https://doi.org/10.3390/F9070398.
Maas, H.-G., Bienert, A., Scheller, S., Keane, E., 2008. Automatic forest inventory parameter determination from terrestrial laser scanner data. Int. J. Remote Sens. 29 (5), 1579–1593. https://doi.org/10.1080/01431160701736406.
Marchi, N., Pirotti, F., Lingua, E., 2018. Airborne and Terrestrial Laser Scanning Data for the Assessment of Standing and Lying Deadwood: Current Situation and New Perspectives. Remote Sens. 10, 1356. https://doi.org/10.3390/RS10091356.
Matsumura, N., Arita, T., Hirose, Y., Numamoto, S., Shimada, H., Nomura, H., 2020. Accuracy validation of various measurement instruments for acquisition of high precision forest resource information. Japanese J. For. Plan. 54, 55–61. https://doi.org/10.20659/jjfp.54.1_55.
Moe, K.T., Owari, T., Furuya, N., Hiroshima, T., Morimoto, J., 2020. Application of UAV Photogrammetry with LiDAR Data to Facilitate the Estimation of Tree Locations and DBH Values for High-Value Timber Species in Northern Japanese Mixed-Wood Forests. Remote Sens. 12, 2865. https://doi.org/10.3390/rs12172865.
Muroki, N., T. I, 2019. Estimating a stand volume using UAV-aerial images and terrestrial laser scanning. Japanese J. For. Plan. 52, 83–88. https://doi.org/10.20659/jjfp.52.2_83.
Nishizono, T., Hosoda, K., Fukumoto, K., Yamada, Y., Takahashi, M., Saito, H., Kitahara, F., Kodani, E., 2020. Effects of stand condition and history on measurement errors for tree size using terrestrial laser scanning in Chamaecyparis obtusa man-made forests. Japanese J. For. Plan. 54, 37–44. https://doi.org/10.20659/jjfp.54.1_37.
Ota, T., Ogawa, M., Shimizu, K., Kajisa, T., Mizoue, N., Yoshida, S., Takao, G., Hirata, Y., Furuya, N., Sano, T., Sokh, H., Ma, V., Ito, E., Toriyama, J., Monda, Y., Saito, H., Kiyono, Y., Chann, S., Ket, N., 2015. Aboveground Biomass Estimation Using Structure from Motion Approach with Aerial Photographs in a Seasonal Tropical Forest. Forests 6, 3882–3898. https://doi.org/10.3390/f6113882.
Polewski, P., Yao, W., Cao, L., Gao, S., 2019. Marker-free coregistration of UAV and backpack LiDAR point clouds in forested areas. ISPRS J. Photogramm. Remote Sens. 147, 307–318. https://doi.org/10.1016/j.isprsjprs.2018.11.020.
Puletti, N., Grotti, M., Ferrara, C., Chianucci, F., 2020. Lidar-based estimates of aboveground biomass through ground, aerial, and satellite observation: a case study in a Mediterranean forest. J. Appl. Remote Sens. 14, 044501. https://doi.org/10.1117/1.JRS.14.044501.
Puletti, N., Grotti, M., Scotti, R., 2019. Evaluating the Eccentricities of Poplar Stem Profiles with Terrestrial Laser Scanning. Forests 10, 239. https://doi.org/10.3390/F10030239.
Puliti, S., Dash, J.P., Watt, M.S., Breidenbach, J., Pearse, G.D., 2019. A comparison of UAV laser scanning, photogrammetry and airborne laser scanning for precision inventory of small-forest properties. For. An Int. J. For. Res. 93, 150–162. https://doi.org/10.1093/forestry/cpz057.
Pyörälä, J., Kankare, V., Liang, X., Saarinen, N., Rikala, J., Kivinen, V.-P., Sipi, M., Holopainen, M., Hyyppä, J., Vastaranta, M., 2019. Assessing log geometry and wood quality in standing timber using terrestrial laser-scanning point clouds. For. An Int. J. For. Res. 92, 177–187. https://doi.org/10.1093/forestry/cpy044.
R Core Team, 2020. R: A Language and Environment for Statistical Computing. R Found. Stat. Comput, Vienna.
Roşca, S., Suomalainen, J., Bartholomeus, H., Herold, M., 2018. Comparing terrestrial laser scanning and unmanned aerial vehicle structure from motion to assess top of canopy structure in tropical forests. Interface Focus 8 (2), 20170038. https://doi.org/10.1098/rsfs.2017.0038.
Roussel, J.-R., Auty, D., Coops, N.C., Tompalski, P., Goodbody, T.R.H., Meador, A.S., Bourdon, J.-F., de Boissieu, F., Achim, A., 2020. lidR: An R package for analysis of Airborne Laser Scanning (ALS) data. Remote Sens. Environ. 251, 112061. https://doi.org/10.1016/j.rse.2020.112061.
Snavely, N., Seitz, S.M., Szeliski, R., 2008. Modeling the World from Internet Photo Collections. Int. J. Comput. Vis. 80 (2), 189–210. https://doi.org/10.1007/s11263-007-0107-3.
Suematsu, N., Ota, T., Shimizu, K., Fukumoto, K., Mizoue, N., Inoue, A., Kitazato, H., Kusano, H., Kai, H., Omasa, Y., 2020. The influence of sampling grid resolution and understory on forest structure estimation from terrestrial laser scanning. Japanese J. For. Plan. 54, 45–54. https://doi.org/10.20659/jjfp.54.1_45.
Tian, J., Dai, T., Li, H., Liao, C., Teng, W., Hu, Q., Ma, W., Xu, Y., 2019. A Novel Tree Height Extraction Approach for Individual Trees by Combining TLS and UAV Image-Based Point Cloud Integration. Forests 10, 537. https://doi.org/10.3390/f10070537.
Tomppo, E., Gschwantner, T., Lawrence, M., McRoberts, R.E., Gabler, K., Schadauer, K., Vidal, C., Lanz, A., Ståhl, G., Cienciala, E., 2010. National forest inventories. Pathways for Common Reporting. European Science Foundation. Springer.
Tremblay, J.F., Béland, M., 2018. Towards operational marker-free registration of terrestrial lidar data in forests. ISPRS J. Photogramm. Remote Sens. 146, 430–435. https://doi.org/10.1016/J.ISPRSJPRS.2018.10.011.
Tsubouchi, T., 2019. Introduction to Simultaneous Localization and Mapping. J. Robot. Mechatronics 31 (3), 367–374.
Vaglio Laurin, G., Ding, J., Disney, M., Bartholomeus, H., Herold, M., Papale, D., Valentini, R., 2019. Tree height in tropical forest as measured by different ground, proximal, and remote sensing instruments, and impacts on above ground biomass estimates. Int. J. Appl. Earth Obs. Geoinf. 82, 101899. https://doi.org/10.1016/j.jag.2019.101899.
Wang, Y., Lehtomäki, M., Liang, X., Pyörälä, J., Kukko, A., Jaakkola, A., Liu, J., Feng, Z., Chen, R., Hyyppä, J., 2019. Is field-measured tree height as reliable as believed – A comparison study of tree height estimates from field measurement, airborne laser scanning and terrestrial laser scanning in a boreal forest. ISPRS J. Photogramm. Remote Sens. 147, 132–145. https://doi.org/10.1016/J.ISPRSJPRS.2018.11.008.
White, J.C., Coops, N.C., Wulder, M.A., Vastaranta, M., Hilker, T., Tompalski, P., 2016. Remote Sensing Technologies for Enhancing Forest Inventories: A Review. Can. J. Remote Sens. 42 (5), 619–641. https://doi.org/10.1080/07038992.2016.1207484.
Xu, D., Wang, H., Xu, W., Luan, Z., Xu, X., 2021. LiDAR Applications to Estimate Forest Biomass at Individual Tree Scale: Opportunities, Challenges and Future Perspectives. Forests 12, 550. https://doi.org/10.3390/f12050550.
Yrttimaa, T., Saarinen, N., Kankare, V., Liang, X., Hyyppä, J., Holopainen, M., Vastaranta, M., 2019. Investigating the Feasibility of Multi-Scan Terrestrial Laser Scanning to Characterize Tree Communities in Southern Boreal Forests. Remote Sens. 11, 1423. https://doi.org/10.3390/RS11121423.
Zhang, W., Qi, J., Wan, P., Wang, H., Xie, D., Wang, X., Yan, G., 2016. An Easy-to-Use Airborne LiDAR Data Filtering Method Based on Cloth Simulation. Remote Sens. 8, 501. https://doi.org/10.3390/rs8060501.
Zhang, W., Shao, J., Jin, S., Luo, L., Ge, J., Peng, X., Zhou, G., 2021. Automated Marker-Free Registration of Multisource Forest Point Clouds Using a Coarse-to-Global Adjustment Strategy. Forests 12, 269. https://doi.org/10.3390/f12030269.